atmosphere

MDPI

Article

Modeling Greenhouse Gas Emissions from Agriculture

Alina Bărbulescu

Department of Civil Engineering, Transilvania University of Brașov, 5 Turnului Str., 500152 Brașov, Romania; alina.barbulescu@unitbv.ro

Abstract: This study analyzes the series of annual emissions of greenhouse gases (GHGs) from agriculture in the European Union countries for 32 years. The outliers, autocorrelation, and change points were detected for each series and the Total one using the boxplot, autocorrelation function (ACF), and Pettit, Hubert, and CUSUM tests. The existence of a monotonic trend in the data series was checked against the randomness by the Mann–Kendall test; further, the slope of the linear trend was determined by Sen's nonparametric approach and classical regression. The best distribution was fitted for each data series. The results indicate that most series present aberrant values (indicating periods with high emissions), are autocorrelated, and have a decreasing tendency over time (showing the diminishing of GHG emissions from agriculture during the study period). The distributions that best fit the individual series were of Wakeby, Johnson SB, Burr, and Log-logistic type. The Total series has a decreasing trend, presents a second-order autocorrelation, and is right-skewed. An ARIMA(1,1,2) model was built and validated for it and was used for the forecast.

Keywords: GHG; outlier; trend; change point; ARIMA; agriculture

Academic Editors: Jianjun Wang and Xufeng Zheng

Received: 29 January 2025
Revised: 23 February 2025
Accepted: 27 February 2025
Published: 28 February 2025

Citation: Bărbulescu, A. Modeling Greenhouse Gas Emissions from Agriculture. *Atmosphere* **2025**, *16*, 295. https://doi.org/10.3390/atmos16030295

1. Introduction

Agriculture is essential for feeding the global population, but certain agricultural practices contribute significantly to various forms of environmental pollution. The relationship between agricultural practices and pollution is complex. Many farming techniques and activities directly or indirectly lead to water-, soil-, and air-quality degradation [1], as summarized below.

(a) Water pollution is produced by the following:
- Nutrient runoff due to fertilizers (often containing nitrogen and phosphorus) that can wash into rivers, lakes, and oceans during rain, leading to eutrophication [2].
- Pesticides and herbicides, which often find their way into water systems through runoff or leaching, contaminate drinking-water sources and become a possible risk to human life and ecosystems [3].
- Livestock waste, which contains harmful pathogens, excess nutrients, and chemicals that can contaminate water supplies when they are improperly managed [4,5].

(b) Soil pollution is the result of the following:
- Overusing pesticides and synthetic fertilizers that can contaminate soil, reducing soil quality and biodiversity [6].

- Agricultural practices like deforestation, overgrazing, and unsustainable farming methods can lead to soil erosion, degrading the land quality and contributing to sedimentation in waterways, thus harming aquatic habitats [7].

(c) Air pollution appears due to the following:

- Ammonia (NH_3) released into the atmosphere from two main sources—animal manure and synthetic fertilizers—which can cause health issues, especially respiratory problems [8].
- GHGs emitted from livestock farming (that produces methane—CH_4—through enteric fermentation), and fertilizers use (emitting nitrous oxide—N_2O). They are essential contributors to climate change [9], and their effects are mostly irreversible. Apart from burning fossil fuels, CO_2 is mainly produced by microbial activity in the soil and the plants' decay [10].

CH_4 remains approximately 12 years in the atmosphere and traps heat more than 25 times better than CO_2 in the short term [11,12]. N_2O is an important anthropogenic greenhouse gas, and agriculture is its most significant producer [13,14]. Compared to CO_2, N_2O has a global-warming potential that is 310 times greater over 100 years, persisting in the atmospheric environment for approximately 109 years and significantly contributing to climate change on the long-range horizon [15].

The FAO report [16] comprehensively analyzes livestock's contribution to GHG emissions and identifies mitigation strategies, mainly focusing on methane from enteric fermentation. Using life cycle assessment, statistical analysis, and scenario modeling, it also estimates the sector's mitigation potential and highlights specific options for reducing emissions. Hristov et al. [17] review strategies to mitigate methane emissions from livestock, such as feed additives, breeding for lower methane-emitting animals, and improved livestock management.

Various models for the emission process were also proposed. For example, Nikolaisen et al. [18] proposed a GAM model for the emissions of CH_4 from rice paddies, considering as variables the soil organic carbon, pH, water regime during the growing season, crop duration, and organic amendment. They also suggested possible mitigation strategies, such as water management (alternate wetting and drying) and the use of methanotrophic bacteria. The article [19] presents a comparison of the models proposed in [20,21] for the same conditions. Cheng et al. [22] and Begum et al. [23] used the DayCent model to simulate the GHG mitigation possibility in China and Bangladesh, respectively. In the same category as DayCent are the following process models for grassland, livestock, and crop: APSIM, DNDC, EPIC-APEX, NASA-CASA, Roth-C, and RUMINANT [24]. A review of various types of models (DairyWise, FarmGHG, FarmSim, GLEAM, SIMS-Diary, IFSM, IMAGE, LEITAP, and MITERRA) for the emission of different GHGs from livestock is provided in [25]. Still, none of the mentioned articles considers the GHG emission series; instead, they cover their emission mechanism and the factors that influence it.

The spatiotemporal patterns of different types of methane emissions were also determined [26]. The scientists indicate that it is critical to understand the laws governing the emission process in order to be able to take measures for pollution reduction from agriculture, as proposed in [27].

The factors favoring the N_2O emissions from agricultural soils are discussed in [28,29], whereas the options for their reductions and the costs involved are presented in [30]. Given the effort of diminishing pollution with GHG from agriculture, various solutions have been proposed [22,31–34]. According to Smith et al. [35], the most significant impact in this direction is enhancing cropland and grazing-land management, restoring degraded lands, and cultivating organic soils. Water and rice management, land use

changes, agroforestry, manure, and livestock management also play an important role in achieving this goal.

Whereas a projection for 2050 indicates 1.7 gigatons of GHG emissions from agriculture [36], the European Union (EU) targets the reduction of CO_2 emissions by 55% by 2030 and aims to achieve climate neutrality by 2050 [37]. Considering this goal, the novelty of this research is to provide a deep investigation of the evolution of the GHG emissions series from agriculture in the EU countries from 1990 to 2022, including their trend (increasing or decreasing) and the distributions that better characterize them. The attempt is important for a future forecast of the series' tendency in the pursuit of reaching the EU objective.

We also propose an ARIMA model describing the total GHG emissions from agriculture in the EU. This model is used for forecasting the data series. The research extends the results from [38,39] and represents the basis for predicting agricultural GHG series evolution as a significant background for evaluating the stage of achieving the EU directives.

The rest of the article is structured as follows: Section 2—Materials and Methods—contains the data series and the methodology, including the statistical methods used to determine the series characteristics and the modeling technique. Section 3—Results and Discussion—presents the results of the analysis of the individual series, their distributions, and the ARIMA model for the Total series. Section 4—Conclusions—summarizes the study's findings.

2. Materials and Methods

The data series consists of the annual GHG emissions from agriculture in the UE countries from 1990 to 2022 (Figure 1), downloaded from [40], whereas Figure 2 presents the volumes of GHG (in thousand tons) emitted in 2022, generated from [41].

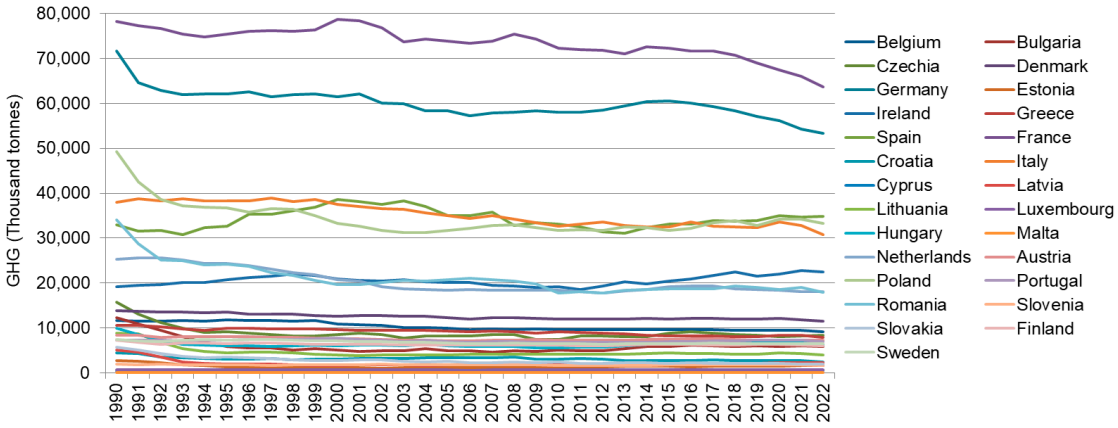

Figure 1. Volume of GHG emissions from agriculture in the EU countries from 1990 to 2022 (processed from the data available in [40]).

Statistical analysis of the data series consisted of the following:

i. Determining the boxplots and the outlying values.

In this study, boxplots were built considering the quartiles and the interquartile range (*IQR*, i.e., difference between the upper quartile (Q_3) and the lower quartile (Q_1)). The outliers (aberrant values) are the values greater than $Q_3 + 1.5 \times IQR$ or lower than $Q_1 - 1.5 \times IQR$ [42].

ii. Investigating the autocorrelation in each series.

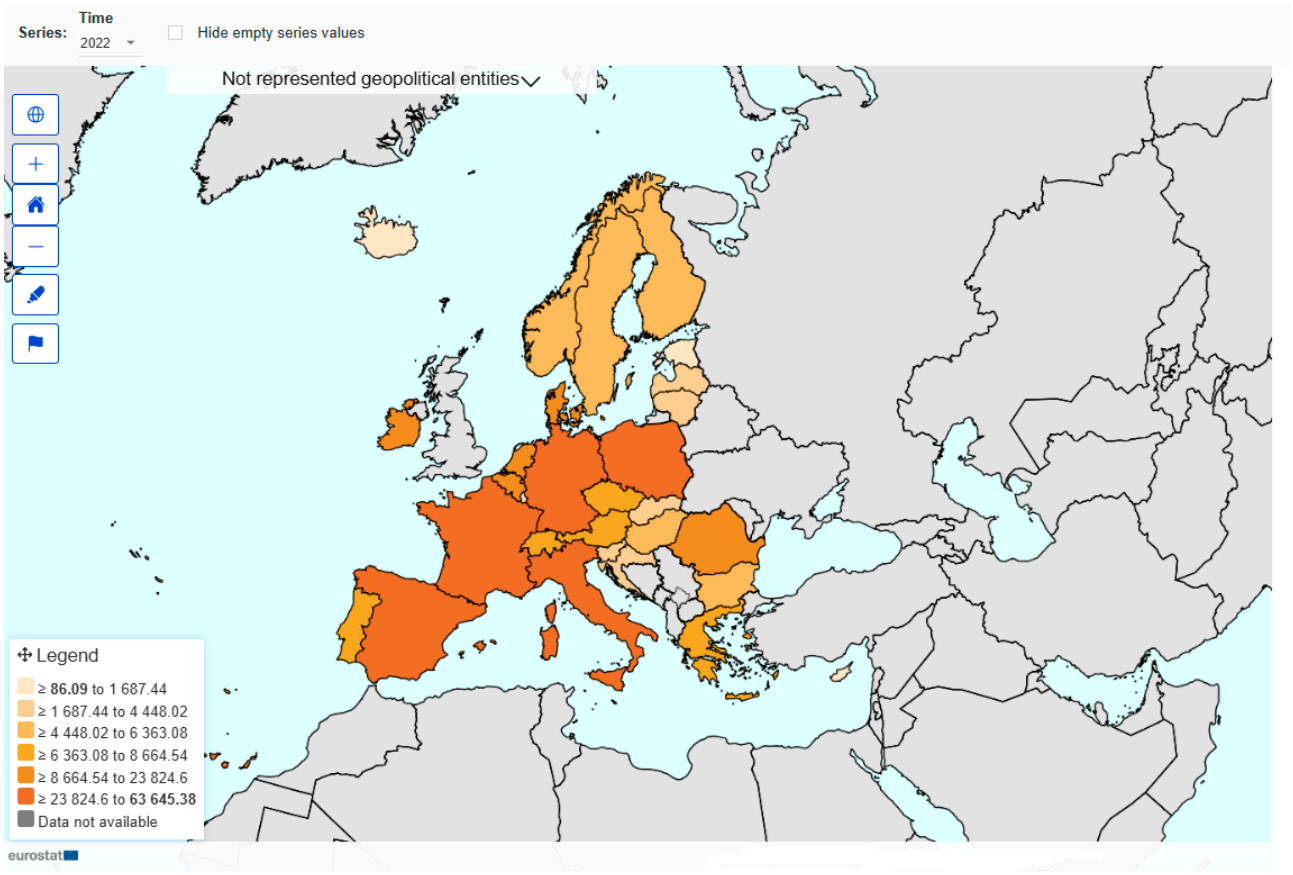

Figure 2. Volume of GHG emissions from agriculture in 2022 [41].

ACF indicates the variation in the correlation between two series values when the distance (lag) between them is modified [43]. For a time-series process, X_t, ACF is defined by the following:

$$\rho_h = \frac{\mathrm{Cov}(X_t, X_{t+h})}{\sqrt{\mathrm{Var}(X_t)\mathrm{Var}(X_{t+h})}}, \quad (1)$$

where $\mathrm{Cov}(X_t, X_{t+h})$ is the covariance of X_t and X_{t+h}, and $\mathrm{Var}(X_t)$ is the variance of X_t.

ACF measures the process memory. In our case, the series autocorrelation indicates the persistence of pollution over a certain period and the fact that the previous values influence the values recorded at a particular moment. To address this, we draw the correlograms and empirical confidence intervals at a 95% confidence level. The autocorrelation hypothesis cannot be rejected if there are ACF values outside the confidence interval.

iii. Investigating the change points existence.

This analysis was performed by various techniques. The classical Pettitt test [44,45] determined a single change point for each series, whereas the Hubert [46] and CUSUM [47] tests were utilized to detect multiple break points. Given the autocorrelation of the residuals in the model on which the CUSUM is based, this procedure could not be performed for all series, as shown in Table 2, column 6. The change points are listed based on their importance as they were detected by the method implemented in the Change-Point Analyser 2.3 (https://variation.com/product/change-point-analyzer/ (accessed on 10 February 2025)).

iv. Analyze the existence of a decreasing trend in the data series.

Two methods were used to detect the existence of such a trend for each data series. The first one was fitting a linear parametric model of the GHG volume as a function of time. The significance of the coefficients was tested by the *t*-test, and that of the model as a whole was tested by the F-test. The R^2 was also computed. If the coefficients and the

model were significant, we reported the slope. When it is negative (positive), the trend is decreasing (increasing).

If the coefficients in the parametric model or the model itself were not significant, the Mann–Kendall test was used to test the hypothesis that the series has a monotonic trend against its randomness [48]. Sen's (nonparametric) slope was detected for the linear trend when the randomness was rejected. It must be mentioned that the slope from the deterministic model and Sen's procedure are not equal because of the specific background of each method.

In the following, we call the sum of the series recorded in all the 27 EU countries the Total series.

v. Fit the best distribution for each data series and for the Total one.

For this goal, the Kolmogorov–Smirnov [49], Chi-squared [50], and Anderson–Darling [51] goodness-of-fit tests have been employed. If the results were not concordant, the distribution ranked in a lower position (by summing up the ranks assigned by each criterion) was chosen.

vi. An ARIMA [43,52] model has been proposed for the Total series evolution.

The Box–Jenkins approach has been used because of its flexibility and successful modeling results in various domains for time-series forecast [49,53–55].

Given a time series, $\{Y_t\}$, $t \in \mathrm{N}^*$, an ARIMA(p,d,q) model for it is defined by Equation (1):

$$\left(1 - \varphi_1 B - \cdots - \varphi_p B^p\right)\nabla^d Y_t = \left(1 - \theta_1 B - \cdots - \theta_q B^q\right)\varepsilon_t, \quad (2)$$

where B is the backshift operator; $\varphi_p \neq 0, \theta_q \neq 0, p$ is the autoregressive order; q is the moving average order; d is the degree of differentiation,

$$\nabla^d = (1 - B)^d; \quad (3)$$

and $\{\varepsilon_t\}$ is a white noise with a constant variance and zero mean.

The left side of Equation (2) represents the autoregressive (AR) part of the model, whereas the right-hand side is the innovation part (the moving average part).

Determining the ARIMA model involved the following stages:

i. Analyze the data series, e.g., trend detection, computation of the ACF, and partial autocorrelation function (PACF). PACF indicates the correlation between a stationary time series and its lagged values, after removing the effects of intermediary time steps.

ii. Test the series stationarity using the KPSS test [56]. The null hypothesis is trend (or level) stationarity, and the alternative is the non-stationarity.

$\{Y_t\}$ is called stationary if the expectation of Y_t^2, $\mathrm{E}(Y_t^2)$, is finite, $E(Y_t)$ is constant in time, and, the covariance, $\mathrm{Cov}(Y_t, Y_{t+h})$, does not depend on the time t [52].

iii. If the stationarity hypothesis cannot be rejected, move to step iv. Otherwise, process the data series: take the difference when the trend is linear, and redo the test to check the stationarity of the new series. After reaching the stationarity, move to the next step.

iv. Determine the model's parameters based on the correlogram and the chart of PACF. A peak of PACF is a potential AR term in the model. The PACF's cut-off represents a potential p, whereas the *ACF*'s cut-off is a potential q [52].

v. Select the best model using the Akaike criteria: $AIC = -2\ln(L) + 2k$, where k is the number of parameters, and L is the maximum of the likelihood function.
Among the possible models, the best model is that with the smallest AIC [52].

vi. Predict future values based on the built model.

3. Results and Discussion

3.1. Results for Individual Series

We used the abbreviations: Austria—AT; Belgium—BE; Bulgaria—BG; Cyprus—CY; Czech Republic—CZ; Germany—DE; Denmark—DK; Estonia—EE; Spain—ES; Finland—FI; France—FR; Greece—GR; Croatia—HR; Hungary—HU; Ireland—IE; Italy—IT; Luxembourg—LU; Lithuania—LT; Latvia—LV; Malta—ML; Netherlands—NL; Poland—PL; Portugal—PT; Romania—RO; Sweeden—SE; Slovenia—SI; and Slovakia—SK.

i. To give an image of the extent of GHG emissions during the study period, Figure 3 presents the boxplots of the study series. BG, CZ, DE, EE, FI, FR, HR, HU, LT, LV, PL, RO, and SK series have outliers, represented by stars, indicating the existence of years with very high GHG emissions. Moreover, we can differentiate between the high-emitters—FR and DE; medium emitters—ES, PL, NL, RO, and IE; and all the other countries, which are much lower polluters.

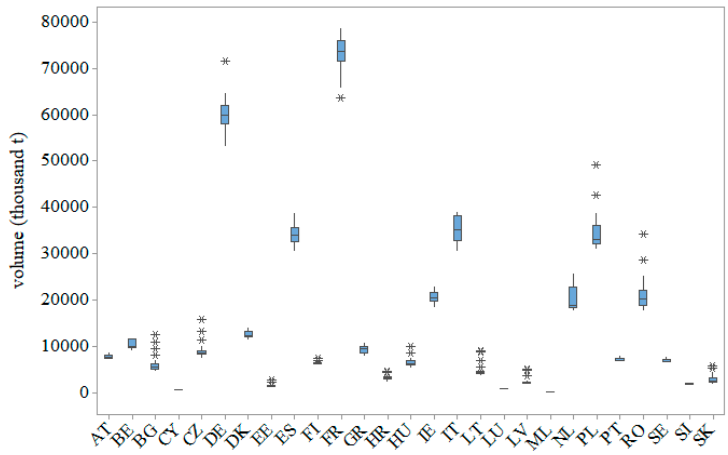

Figure 3. Boxplots of the study series. The stars represent the outliers.

ii. The ACF's analysis indicated that all series present autocorrelation. Figure 4 contains the AT, IT, and FI series correlograms with a 95% confidence interval.

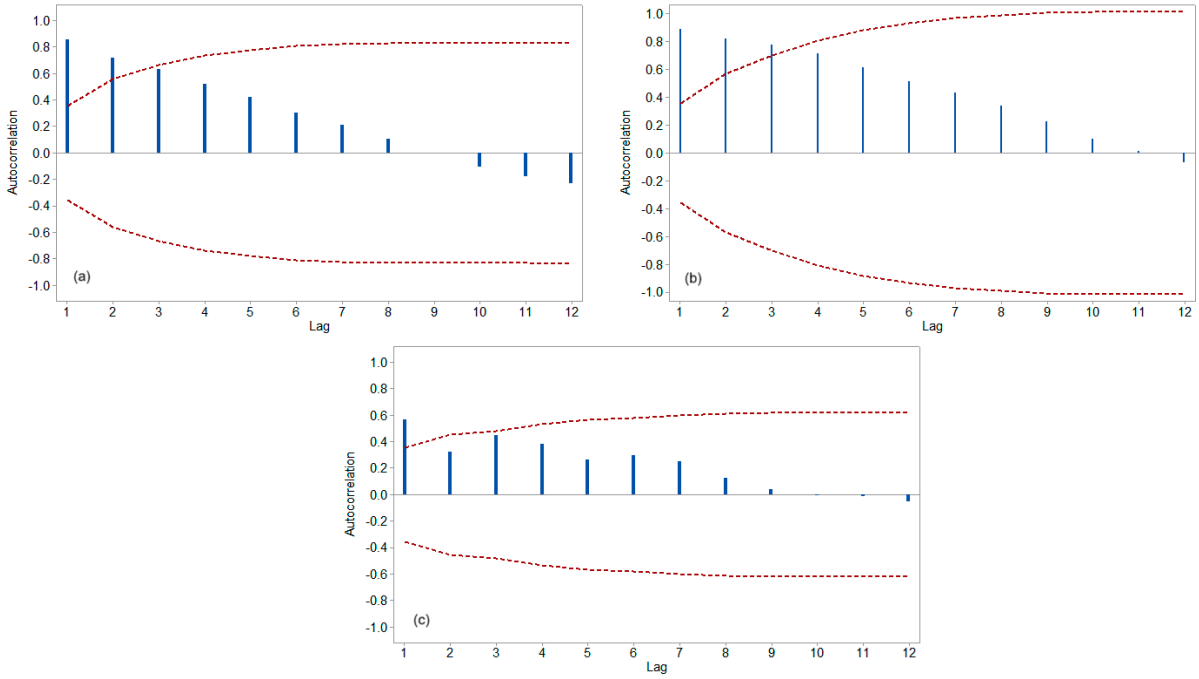

Figure 4. ACF for (**a**) AT, (**b**) IT, and (**c**) FI series with a 95% confidence interval.

The ACF's values are represented by the vertical bars, and the dotted red curve represents the confidence interval limits. AT has a second-order autocorrelation because two values of ACF are outside the confidence interval, whereas IT (FI) has third- (first-) order autocorrelation.

The third column of Table 1 indicates the autocorrelation order for each series. Summarizing, 9, 12, and 6 series present first-order, second order, and third-order autocorrelation, respectively, indicating the accumulation of the pollutants in the atmosphere.

Table 1. Autocorrelation, **c**hange points, and the distribution fitted for each series.

No.	Series	Autocorrelation Order	Change Points		
			Pettitt	Hubert	CUSUM
1	AT	2	13	3, 10, 13	-
2	BE	3	16	11, 14, 17	11, 14, 17
3	BG	2	8	2, 4, 5, 9	5, 25
4	CY	2	18	4, 19	-
5	CZ	1	8	2, 3, 5	-
6	DE	1	13	2, 13	-
7	DK	3	8	7, 10, 15, 20	-
8	EE	1	6	3, 4, 6, 23	-
9	ES	2	-	7, 19	7, 10, 16, 19, 28
10	FI	1	13	2, 10	16
11	FR	2	13	14, 21, 30	-
12	GR	3	15	4, 11, 19, 25	4, 11, 19, 25
13	HR	1	19	3, 24	3, 15, 20, 24
14	HU	1	24	2,3,5,26	-
15	IE	2	-	6, 15, 27	-
16	IT	3	15	11,15,20	11, 15, 20
17	LT	1	9	3,4,5,10	-
18	LU	2	11	13, 26	13, 19, 26
19	LV	1	8	3,4	-
20	ML	3	15	11, 15, 20	-
21	NL	2	13	5, 8, 13	-
22	PL	1	11	2, 3, 11	-
23	PT	2	15	16, 28	-
24	RO	2	19	2, 3, 7, 10	-
25	SE	3	16	10, 16	10,16
26	SI	2	14	7,19	7, 11, 14, 21, 26
27	SK	2	16	3, 4, 9, 16	4,15, 28

iii. The three methods have found various change points. While the Pettitt test indicated when the most probable change point is likely to appear, the other two procedures either found at least two such points or could not be performed due to the deviation from the hypothesis they rely on (this is the case of CUSUM).

In most cases when both Hubert and CUSUM tests could be performed, common change points were found. Comparing the results of the Pettitt and Hubert test, we found that the predominant breakpoint (Pettitt) either corresponds with one of the change points found by the Hubert procedure (in turquoise in Table 1) or is in the neighborhood (e.g., for PT, 15 by Pettit, and 16 for Hubert).

Given the various methodologies on which the tests are based, a perfect match between the results of these three tests was not expected. Still, the fact that each series has at least a break point indicates a significant modification in the average GHG series after the change-point moment with respect to the average before it.

iv. After examining the data series visually, we fit a linear model for each series' evolution in time (so, the independent variable was time, and the dependent variable was the volume of GHG emissions from agriculture) to address whether pollution tendency was to diminish or increase during the study period. Column 2 of Table 2 contains the slopes in the linear trends determined by the parametric procedure of the least squares method and the corresponding determination coefficients (R^2) inside the brackets.

Table 2. Slopes of the linear trend determined by the parametric (least squared method) and nonparametric (Sen's slope) methods.

No.	Country	Slope of the Linear Parametric Trend and R^2 (Inside Bracket)	Sen's Slope and *p*-Value (Inside Bracket)
1	AT	−28.6255 (60.89%)	−28.2904 (<0.0001)
2	BE	−86.7240 (84.54%)	−79.4657 (<0.0001)
3	BG	−81.0714 (20.06%)	−10.2054 (0.6985)
4	CY	Model not significant	−1.2258 (0.1777)
5	CZ	−90.2248 (28.98%)	−37.9688 (0.0050)
6	DE	−266.5380 (62.61%)	−249.4031 (<0.0001)
7	DK	−62.1136 (87.97%)	−63.7738 (<0.0001)
8	EE	Model not significant	8.5937 (0.1496)
9	ES	Model not significant	8.8672 (0.8891)
10	FI	−18.6326 (52.15%)	−15.6786 (<0.0001)
11	FR	−312.4920 (75.09%)	−284.375 (<0.0001)
12	GR	−73.6078 (94.46%)	−72.86611 (<0.0001)
13	HR	−32.8327 (58.02%)	−27.2886 (<0.0001)
14	HU	Model not significant	4.7892 (0.7685)
15	IE	Model not significant	38.6600 (0.1038)
16	IT	−249.6000 (98.42%)	−252.2263 (<0.0001)
17	LT	−68.2652 (29.61%)	−11.9541 (0.1679)
18	LU	Model not significant	−0.7542 (0.0973)
19	LV	−30.4156 (14.89%)	10.4355 (0.1496)
20	ML	−1.1150 (85.47%)	−1.1163 (<0.0001)
21	NL	−236.0144 (71.36%)	−231.2398 (<0.0001)
22	PL	−236.0796 (38.29%)	−153.6965 (0.0097)
23	PT	−14.3618 (29.33%)	−14.8273 (0.0061)
24	RO	−281.3051 (61.70%)	−219.9531 (<0.0001)
25	SE	−32.7583 (77.40%)	−4.3634 (<0.0001)
26	SI	−4.8368 (46.20%)	−32.7668 (<0.0001)
27	SK	−76.7572 (69.74%)	−57.4438 (<0.0001)

The significance of the parameters in the model (slope and intercept) was tested by the *t*-test, whereas the F-test was performed to verify the model's significance. When the model was not significant (the *p*-value of the F-test for the model significance was greater than 0.05—the significance level), we filled in Table 2 with "Model not significant".

Given that the linear parametric models for CY, EE, ES, HU, IE, and LU series were found to be non-significant, and R^2 was very small for other models (BG, CZ, LT, LV, PL, PT, and SI), we applied the MK test, followed by the nonparametric Sen's procedure to assess the existence of a decreasing trend of each individual series. The Sen's slopes and the *p*-values (inside the brackets) are found in the last column of Table 2. A *p*-value less than 0.05 indicates a significant slope.

The MK test did not confirm the existence of a significant monotonic trend for CY, EE, ES, HU, IE, LU, BG, LT, and LV (*p*-values > 0.05). For CZ, PL, PT, and SI, they

confirmed the existence of a decreasing trend (p-values < 0.05, and the corresponding z-scores—not listed here—are negative).

Performing the same analysis for the period after the change point detected by the Pettitt method and the last change point found by the Hubert procedure, the hypothesis that there is no trend could not be rejected for CY, HU, IE, and LU. A decreasing trend was found for BG, and an increasing one was found for EE, ES, LT, and LV. So, in the most recent period, EE, ES, LT, and LV experienced pollution augmentation, whereas no pollution decrease was noticed in CY, HU, IE, and LU.

v. Table 3 contains the best distributions fitted for each series.

Table 3. Distributions for the studied series.

No.	Series	Distribution Type	Parameters
1	AT	Wakeby	α = 468.81, β = 0.12802, γ = 0, δ = 0, ξ = 7170.8
2	BE	Log-logistic (3p)	α = 2.0921, β = 954.25, γ = 9069.6
3	BG	Log-logistic (3p)	α = 1.578, β = 786.35, γ = 4628.1
4	CY	Wakeby	α = 262.67, β = 2.4572, γ = 7.7626, δ = 0.3875, ξ = 427.07
5	CZ	Wakeby	α = 43,469.0, β = 30.709, γ = 424.2, δ = 0.53181, ξ = 6618.7
6	DE	Johnson SB	γ = −0.88026, δ = 1.7234, λ = 4072.1, ξ = 57,376.0
7	DK	Burr	k = 0.15628, α = 118.94, β = 11,892.0
8	EE	Wakeby	α = 601.18, β = 3.3156, γ = 146.65, δ = 0.39334, ξ = 1085.5
9	ES	Johnson SB	γ = 0.55243, δ = 0.89958, λ = 10,158.0, ξ = 30,386.0
10	FI	Wakeby	α = 34,358.0, β = 73.525, γ = 176.17, δ = 0.18494, ξ = 5688.7
11	FR	Wakeby	$\alpha = 1.5485 \times 10^5$, β = 15.529, γ = 6854.9, δ = −0.76949, ξ = 60,279
12	GR	Johnson SB	γ = −0.09028, δ = 0.88826, λ = 3275.6, ξ = 7481.8
13	HR	Wakeby	α = 1551.4, β = 2.1665, γ = 67.241, δ = 0.54782, ξ = 2504.6
14	HU	Wakeby	α = 11,285.0, β = 20.593, γ = 472.66, δ = 0.28557, ξ = 5260.8
15	IE	Johnson SB	γ = 0.42233, δ = 1.0066, λ = 5437.7, ξ = 18,305.0
16	IT	Frechet	α = 14.976, β = 33,858.0
17	LT	Log-logistic	α = 2.2218, β = 509.44, γ = 3753.3
18	LU	GEV	k = −0.52367, σ = 28.652, μ = 670.77
19	LV	Wakeby	α = 1399.6, β = 8.1012, γ = 210.83, δ = 0.51505, ξ = 1615.1
20	ML	Wakeby	α = 23.88, β = 0.47147, γ = 0, δ = 0, ξ = 79.431
21	NL	Frechet (3p)	α = 1.2358, β = 1153.5, γ = 17486.0
22	PL	Burr	k = 0.15628, α = 118.94, β = 11892.0
23	PT	Inverse Gaussian (3p)	λ = 3037.6, μ = 3529.7, γ = 30,798.0
24	RO	Wakeby	α = 4061.0, β = 7.0628, γ = 2431.2, δ = 0.1862, ξ = 17,525.0
25	SE	Burr	k = 0.02475, α = 670.18, β = 6411.0
26	SI	Burr	k = 0.35268, α = 83.442, β = 1737.5
27	SK	Log-logistic (3p)	α = 1.7925, β = 571.29, γ = 1902.3

Most PDFs are of Wakeby, Johnson SB, and Log-logistic types and are right-skewed. Once again, inhomogeneity between the various series is noticed, indicating a different pattern in the emissions series evolution. This finding is important for modeling the volume of GHG emission series at the regional scale and determining the best spatiotemporal model for pollutant series spread in the UE. We shall not insist on this topic, as it is the subject of another study.

Figure 5 shows the probability density function (PDF) chart of the Wakeby type fitted for HR.

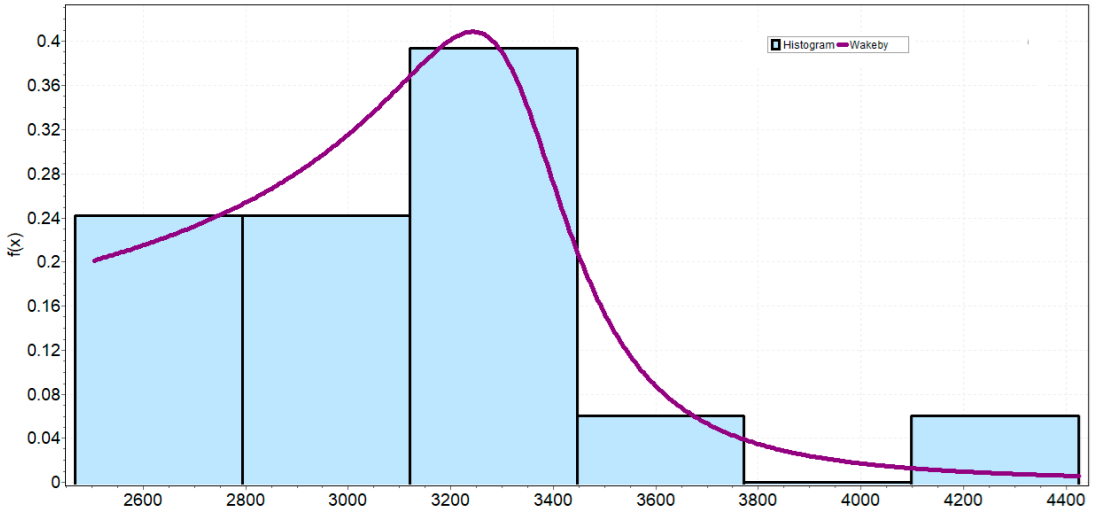

Figure 5. The probability density functions and histograms for HR.

3.2. Results for the Total Series

i. The boxplot of the Total series indicates the existence of a single outlier in 1990, represented by stars in Figure 6a, and a median value between 375,000 and 400,000 megatons.

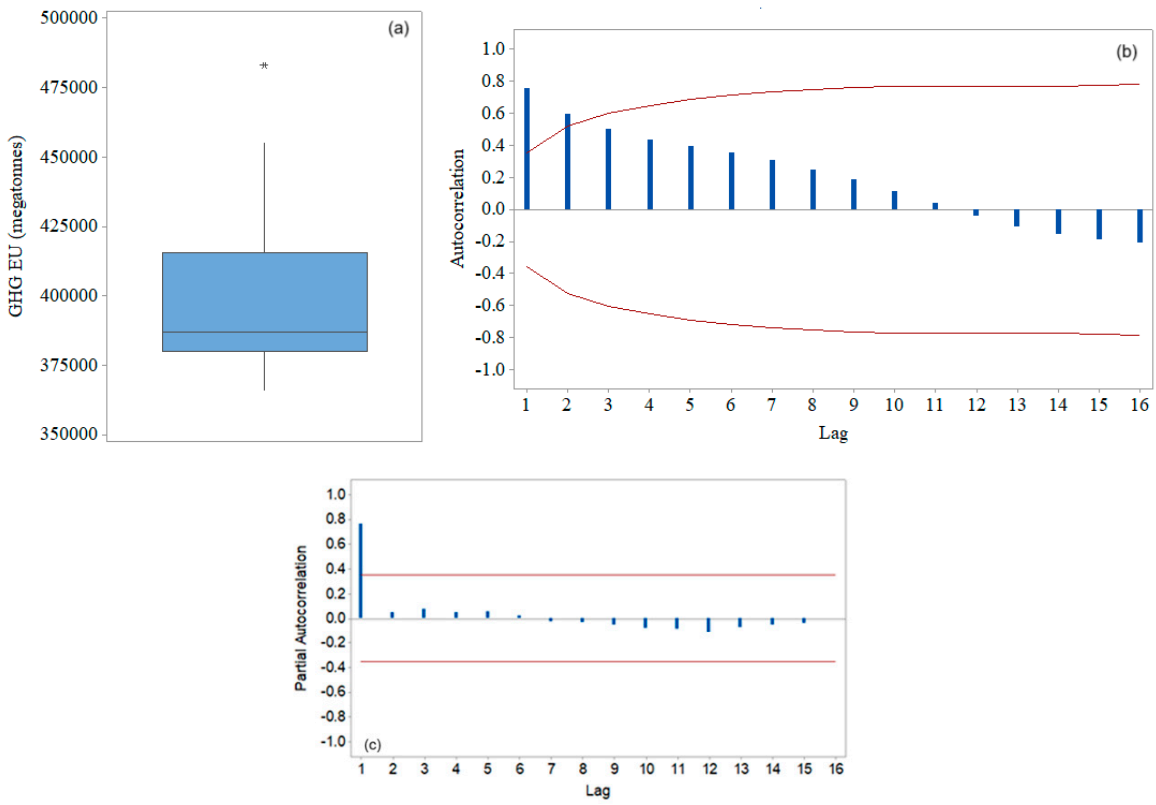

Figure 6. (**a**) Boxplots of the Total series. The stars represent the outliers, (**b**) ACF, and (**c**) PACF of the Total series. The blue bars represent the values of ACF (in (**b**)) and PACF (in (**c**)) at different lags, and the red lines are the limits of the confidence interval with 5% significance level.

ii. Figure 6(b) shows the ACF chart, and Figure 6c contains the chart of PACF. The limits of the confidence interval at a significance level of 5% are represented by red curves. A second-order autocorrelation and a first-order partial autocorrelation are observed. The decreasing shape of ACF can indicate a non-stationarity of the data series, which

will be later addressed. ACF and PACF level off after the second and first lag, respectively (i.e., all the values are inside the confidence interval). This property will be used to determine the parameters for the ARIMA model, as explained in Section 2.

iii. The Pettitt test indicates the 16th year (2005) as a change point, and the Hubert procedure returned the 12th and 19th years (2001 and 2008). The CUSUM hypotheses were violated, so the test was not performed.

iv. After fitting a linear deterministic model for the time series, we found a significant decreasing slope of (–2256.81), with a corresponding variance explained by the model of 74.19%. The MK test confirmed the existence of a significant monotonic trend, with the Sen's slope of (−2128.652 and a p-value < 0.0010). Both procedures indicated a decrement in the volume of GHG emissions from agriculture at the EU level during the study period.

v. Three criteria were utilized to detect the best distribution that can be fit for the Total series. The Johnson SB distribution belongs to the same class of distributions as Johnson SU, normal, and log-normal. Every element of this class could be transformed into a Gaussian distribution by elementary transformations (e.g., $1/x$, sin, exp, ln, arccos, and radical) [57,58].

The equation of the probability distribution function—Johnson SB—fitted for the Total series is as follows:

$$f(x) = \begin{cases} \dfrac{\delta}{\sqrt{2\pi}} \dfrac{\lambda}{(x-\xi)(\xi+\lambda-x)} \exp\left\{-\dfrac{1}{2}\left[\gamma + \delta \ln\left(\dfrac{x-\xi}{\xi+\lambda-x}\right)\right]^2\right\}, \text{if (5)} \\ 0 \qquad\qquad \text{, otherwise} \end{cases} \tag{4}$$

where

$$\xi < x < \xi + \lambda, \delta > 0, -\infty < \gamma < +\infty, \lambda > 0, \xi \geq 0. \tag{5}$$

The parameters are, in this case, as follows:

$$\gamma = 2.1063,\ \delta = 1.0534,\ \lambda = 218520,\ \xi = 36{,}4610. \tag{6}$$

This PDF is represented in Figure 7 by the blue curve, and the histogram of the data series is represented by blue rectangles. The PDF is right-skewed, indicating a higher frequency of the lower values with respect to the higher ones.

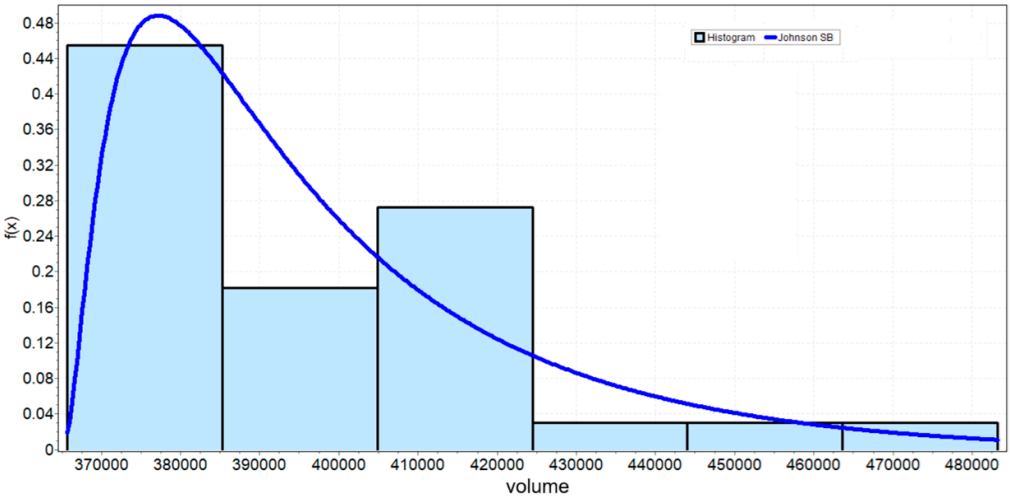

Figure 7. The histogram of the Total series (blue rectangles) and the chart of the Johnson SB theoretical PDF (blue curve).

vi. After analyzing the shape of the data series and its characteristics (trend and autocorrelation), we found that there are no abrupt changes in series evolutions. Moreover,

the existence of a decreasing linear trend determined by the Mann–Kendall and Sen's slope indicates that Box–Jenkins techniques (including ARIMA) can be successfully used, given that they provided good results on modeling time series with similar characteristics from various scientific fields [59–62]. Moreover, the existing implementation of such algorithms in various software helps evaluate the modeling results.

Before fitting the ARIMA model, the series was tested for trend and level stationarity against the unit root hypothesis, using the KPSS test. Since the stationarity hypothesis was rejected, we took the first-order difference to stationarize the series and performed the tests again.

Analyzing the ACF and PACF shapes and the lag where these functions level off, we set $p = 1$ and $q = 2$ in the ARIMA model, whose equation was determined to be as follows:

$$(1 + 0.363B)(1 - B)Y_t = (1 - 576.805B)\varepsilon_t. \quad (7)$$

The model validation involved proving that the residual is a white noise. Figure 8(a) shows that the normality hypothesis could not be rejected by the Ryan–Joiner test [63] because the p-value is greater than 0.100 > 0.05 (which is the significance level).

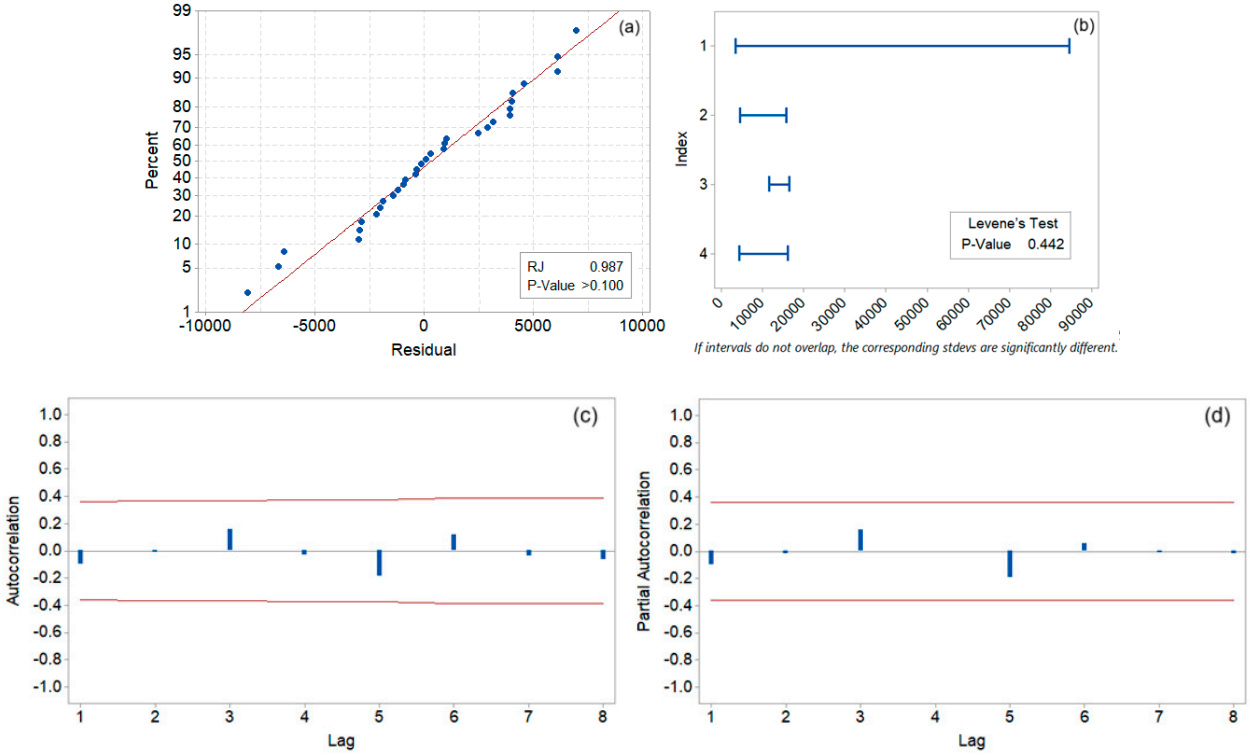

Figure 8. Results of (**a**) the Ryan–Joiner normality test, (**b**) the Levene test for homoscedasticity, (**c**) ACF, and (**d**) PACF of the residual in the model ARIMA(1,1,2).

The Levene homoscedasticity test [64] was performed by dividing the residual series into four sets and comparing their variance. Figure 8(b) indicates that the associated p-value was 0.442 > 0.05, so the homoskedasticity hypothesis could not be rejected. Based on Figure 8(c), (d), we remark that the residual series is not correlated or partially autocorrelated. Therefore, the residual is homoscedastic, Gaussian, independent, and identically distributed. Therefore, the model is validated from a statistical viewpoint.

Based on model (7), forecasts were made on known data series, starting with the 16th year (2005) to 2023 (Figure 9(a)), and for a future period of 5 years, starting from 2023 (Figure 9(b)).

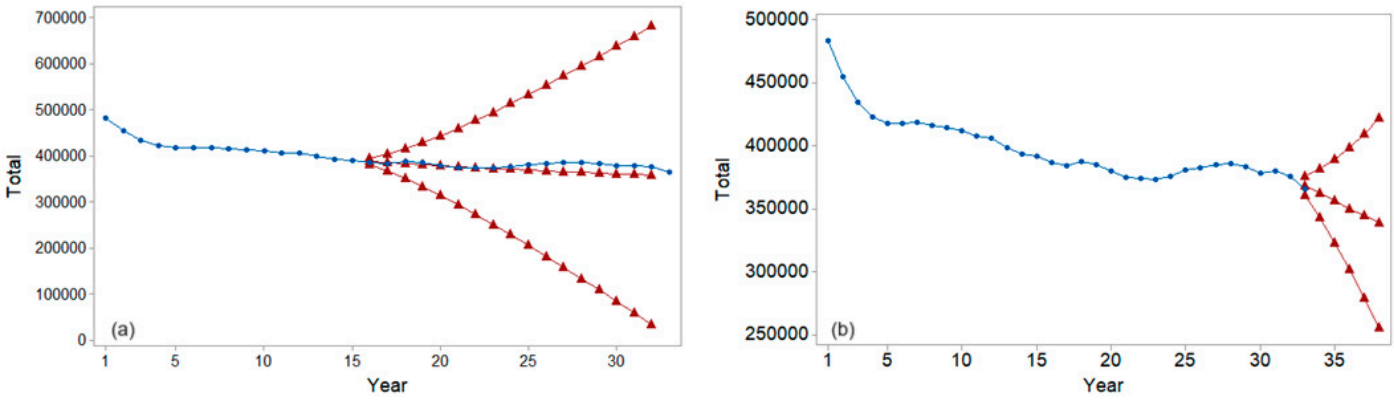

Figure 9. The Total series (blue), the forecast (central red curve), and the limits of the confidence interval (the two divergent lateral curves): (**a**) forecast starting the 16th year (2005) for 17 years; and (**b**) forecast for the future 5 years, starting from 2023.

For the first period, the forecast is represented by the red curve near the blue one (formed by the actual data series in Figure 9a), showing a good fit of the recorded values. This procedure validates the prediction quality provided by the model on the known values of the series. For the second period, the forecast provided future (unknown) values and was built based on the entire series. Since the model was validated from the statistical viewpoint and verified in the first case, we consider the forecast for the future reliable. Figure 9b indicates a decreasing trend of pollution with GHGs from agriculture from 2023 to 2028. In this figure, the predicted values are represented by the central brown curve, and the confidence interval limits are represented by the other two brown curves.

Comparisons of the results of the actual study with those related to the evolution of the CO_2 emission and GHG from all sources in Europe [38,39], lead to the following conclusions:

- The trend of GHG emissions from agriculture recorded a significant decrease in 18 countries out of 27, but no significant increase was noticed for the entire period in any country. By comparison, the study of the CO_2 series from all sources in the EU indicates an increasing tendency in the AT and CY series and non-significant trends in nine countries.
- The change points of the CO_2 series in Europe and the GHG series from agriculture are different. In the first case, one significant change point was found (2003), while in the second one, at least two change points were found (2001 and 2005).
- There was a significant decay in the slope of the Total GHG series from agriculture in 1990–1993 and a slight increase between 2003 and 2007, after which a significant new decrease happened.
- Countries like FR, IT, DE, and NL, where the highest volume of GHG emissions from agriculture was recorded, made the most significant progress in pollution reduction, with the most significant negative slope of the trend.
- ES, an important GHG polluter, made no significant progress in reducing these emissions in general and from agriculture in particular.

4. Conclusions

This study examined the series of GHG emissions from agriculture recorded in EU countries from 1990 to 2023. Significant differences were found across countries, reflected by the fitted distributions, which are mostly right skewed. Based on the determined distribution, the extreme in GHG volume can be easily addressed, and the return period can be also detected.

The results of the Mann–Kendall test emphasize the progress of 18 countries in reducing pollution from this source and a non-significant trend of the rest. The highest polluters made the most significant progress (expressed as the slope of the trend) by diminishing their contribution to the total volume of emissions.

The results indicate that despite decreasing GHG emissions from agriculture at the regional level over the last decade, a third of the UE countries must implement measures to significantly reduce these emissions and achieve the UE directive's goals.

One of the novelties of the article was building an ARIMA model for the Total GHG series. Given the series' statistical characteristics, especially the existence of a linear trend, this technique was appropriate for this purpose. The model was validated on the actual data series before being used to forecast future values of the Total series. The approach can be also utilized for the individual series for which a significant decreasing trend was determined for the entire study period. Moreover, the forecast based on validated models can be successfully utilized to provide precise estimations of the amount of GHG when the conditions on which the models were built are preserved. Still, any potential change in the series' evolution will impact the prediction.

Another advantage of the proposed methodology is its ease of use, given that freeware software with specific packages can be employed.

A limitation of the presented approach is that it does not individually consider the emissions from subsectors of agriculture (but their total), which can impact the modeling accuracy. Therefore, future research should address this issue, model each type of GHG separately, and utilize an aggregation method that will diminish the uncertainty in the modeling. Various other methods, such as those based on the artificial intelligence algorithm, should be utilized to improve forecast accuracy.

Funding: This research received no external funding.

Institutional Review Board Statement: Not applicable.

Informed Consent Statement: Not applicable.

Data Availability Statement: Data are available at https://ec.europa.eu/eurostat/data-browser/view/env_air_gge__custom_12556357/default/table?lang=en (accessed on 10 January 2025)

Conflicts of Interest: The author declares no conflicts of interest.

References

1. Viana, C.M.; Freire, D.; Abrantes, P.; Rocha, J.; Pereira, P. Agricultural land systems importance for supporting food security and sustainable development goals: A systematic review. *Sci. Total Environ.* **2022**, *803 Part 3*, 150718.
2. Madjar, R.M.; Vasile Scăețeanu, G.; Sandu, M.A. Nutrient Water Pollution from Unsustainable Patterns of Agricultural Systems, Effects and Measures of Integrated Farming. *Water* **2024**, *16*, 3146.
3. Syafrudin, M.; Kristanti, R.A.; Yuniarto, A.; Hadibarata, T.; Rhee, J.; Al-Onazi, W.A.; Algarni, T.S.; Almarri, A.H.; Al-Mohaimeed, A.M. Pesticides in Drinking Water-A Review. *Int. J. Environ. Res. Public Health* **2021**, *18*, 468.
4. Zhou, W.; Li, M.; Achal, V. A comprehensive review on environmental and human health impacts of chemical pesticide usage. *Emerg. Contam.* **2025**, *11*, 100410.
5. Dufour, A.; Bartram, J.; Bos, R.; Gannon, V. *Animal Waste, Water Quality and Human Health*; IWA: London, UK, 2012.
6. Aktar, M.W.; Sengupta, D.; Chowdhury, A. Impact of pesticides use in agriculture: Their benefits and hazards. *Interdiscip. Toxicol.* **2009**, *2*, 1–12.
7. Montgomery, D.R. Soil erosion and agricultural sustainability. *Proc. Natl. Acad. Sci. USA* **2007**, *104*, 13268–13272.
8. Merl, T.; Koren, K. Visualizing NH3 emission and the local O2 and pH microenvironment of soil upon manure application using optical sensors. *Environ. Int.* **2020**, *144*, 106080.
9. Chataut, G.; Bhatta, B.; Joshi, D.; Subedi, K.; Kafle, K. Greenhouse gases emission from agricultural soil: A review. *J. Agric. Food Res.* **2023**, *11*, 100533.

10. Greenhouse Gas Cycles in Agriculture. Available online: https://agriculture.vic.gov.au/climate-and-weather/understanding-carbon-and-emissions/greenhouse-gas-cycles-in-agriculture#h2-1 (accessed on 23 January 2024).
11. Climate Change 2021: The Physical Science Basis. Available online: https://www.ipcc.ch/report/ar6/wg1/ (accessed on 23 January 2024).
12. Tian, H.; Xu, R.; Canadell, J.G.; Thompson, R.L.; Winiwarter, W.; Suntharalingam, P.; Davidson, E.A.; Ciais, P.; Jackson, R.B.; Janssens-Maenhout, G.; et al. A comprehensive quantification of global nitrous oxide sources and sinks. *Nature* **2020**, *586*, 248–256.
13. Methane Emissions in the EU: The Key to Immediate Action on Climate Change. Available online: https://www.eea.europa.eu/publications/methane-emissions-in-the-eu (accessed on 23 January 2024).
14. Pan, S.Y.; He, K.H.; Lin, K.T.; Chang, C.-T. Addressing nitrogenous gases from croplands toward low-emission agriculture. *Npj Clim. Atmos. Sci.* **2022**, *5*, 43. https://doi.org/10.1038/s41612-022-00265-3.
15. Reay, D.; Davidson, E.; Smith, K.; Melillo, J.M.; Frank Dentener; Crutzen, P.J. Global agriculture and nitrous oxide emissions. *Nat. Clim. Change* **2012**, *2*, 410–416. https://doi.org/10.1038/nclimate1458.
16. *Tackling Climate Change Through Livestock: A Global Assessment of Emissions and Mitigation Opportunities.* Available online: https://www.fao.org/4/i3437e/i3437e00.htm (accessed on 25 January 2025).
17. Hristov, A.N.; Oh, J.; Lee, C.; Meinen, R.; Montes, F.; Ott, T.; Firkins, J.; Rotz, A.; Dell, C.; Adesogan, A.; et al. Mitigation of Greenhouse Gas Emissions in Livestock Production—A Review of Technical Options for Non-CO_2 Emissions. 2013. Available online: https://www.uncclearn.org/wp-content/uploads/library/fao180.pdf (accessed on 25 January 2025).
18. Nikolaisen, M.; Cornulier, T.; Hillier, J.; Smith, P.; Albanito, F.; Nayak, D. Methane emissions from rice paddies globally: A quantitative statistical review of controlling variables and modelling of emission factors. *J. Clean. Prod*. **2023**, *409*, 137245.
19. Nikolaisen, M.; Hillier, J.; Smith, P.; Nayak, D. Modelling CH_4 emission from rice ecosystem: A comparison between existing empirical models. *Front. Agron*. **2023**, *4*, 1058649.
20. Wang, C.; Lai, D.Y.F.; Sardans, J.; Wang, W.; Zeng, C.; Peñuelas. J. Factors related with CH4 and N2O emissions from a paddy field: Clues for management implications. *PLoS ONE* **2017**, *12*, e0169254.
21. Yan, X.; Yagi, K.; Akiyama, H.; Akimoto, H. Statistical analysis of the major variables controlling methane emission from rice fields. *Glob. Change Biol.* **2005**, *11*, 1131–1141.
22. Cheng, K.; Ogle, S.M.; Parton, W.J.; Pan, G. Simulating greenhouse gas mitigation potentials for Chinese Croplands using the DAYCENT ecosystem model. Glob. Change Biol. **2014**, 20, 948–962.
23. Begum, K.; Kuhnert, M.; Yeluripati, J.; Ogle, S.; Parton, W.; Kader, M.A.; Smith, P. Model Based Regional Estimates of Soil Organic Carbon Sequestration and Greenhouse Gas Mitigation Potentials from Rice Croplands in Bangladesh. *Land* **2018**, *7*, 82.
24. AgLEDx. Available online: https://agledx.ccafs.cgiar.org/estimating-emissions/methods/models/ (accessed on 23 February 2025).
25. Jose, V.S.; Sejian, V.; Bagath, M.; Ratnakaran, A.P.; Lees, A.M.; Al-Hosni, Y.A.S.; Sullivan, M.; Bhatta, R.; Gaughan, J.B. Modeling of Greenhouse Gas Emission from Livestock. *Front. Environ. Sci*. **2016**, *4*, 27.
26. Zhang, B.; Tian, H.; Ren, W.; Tao, B.; Lu, C.; Yang, J.; Banger, K.; Pan, S. Methane emissions from global rice fields: Magnitude, spatiotemporal patterns, and environmental controls. Glob. Biogeochem. Cycles **2016**, 30, 1246–1263.
27. Sakoda, M.; Tokida, T.; Sakai, Y.; Senoo, K.; Nishizawa, T. Mitigation of Paddy Field Soil Methane Emissions by Betaproteobacterium Azoarcus Inoculation of Rice Seeds. *Microbes Environ*. **2022**, *37*, ME22052.
28. Mosier, A.R. Nitrous oxide emissions from agricultural soils. *Fertil. Res.* **1994**, *37*, 191–200.
29. Signor, D.; Eduardo, C.; Cerri, P. Nitrous Oxide Emissions in Agricultural Soils: A Review. Available online: https://www.scielo.br/j/pat/a/yyfWQ9zyWJVdknyBfYFP3wD/?format=pdf&lang=en (accessed on 25 January 2025).
30. Winiwarter, W. Reducing Nitrous Oxide Emissions from Agriculture: Review on Options and Costs. Available online: https://pure.iiasa.ac.at/id/eprint/13396/1/reducing.pdf (accessed on 25 January 2025).
31. Vergé, X.P.C.; De Kimpe, C.; Desjardins, R.L. Agricultural production, greenhouse gas emissions and mitigation potential. *Agric. For. Meteorol*. **2007**, *142*, 255–269.
32. Mitigating GHG Emissions from EU Agriculture—What Difference Does the Policy Make? Available online: https://edepot.wur.nl/239241 (accessed on 25 January 2025).
33. Pricing Agricultural Emissions and Rewarding Climate Action in the Agri-Food Value Chain. Available online: https://www.ecologic.eu/sites/default/files/publication/2023/50109-Pricing-agricultural-emissions-and-rewarding-climate-action-in-the-agri-food-value-chain.pdf (accessed on 25 January 2025).

34. Eash, L.; Ogle, S.; McClelland, S.C.; Fonte, S.J.; Schipanski, M.E. Climate mitigation potential of cover crops in the United States is regionally concentrated and lower than previous estimates. *Glob. Chang Biol*. **2024**, *30*, e17372.
35. Smith, P.; Martino, D.; Cai, Z.; Gwary, D.; Janzen, H.; Kumar, P.; McCarl, B.; Ogle, S.; O'Mara, F.; Rice, C.; et al. Greenhouse gas mitigation in agriculture. *Philos. Trans. R. Soc. Lond. B Biol. Sci*. **2008**, *363*, 789–813.
36. Ntinyari, W.; Gweyi-Onyango, J.P. Greenhouse Gases Emissions in Agricultural Systems and Climate Change Effects in Sub-Saharan Africa. In *African Handbook of Climate Change Adaptation*; Oguge, N., Ayal, D., Adeleke, L., da Silva, I., Eds.; Springer: Cham, Switzerland, 2021.
37. Cutting EU Greenhouse Gas Emissions: National Targets for 2030. Available online: https://www.europarl.europa.eu/topics/en/article/20180208STO97442/cutting-eu-greenhouse-gas-emissions-national-targets-for-2030 (accessed on 25 January 2025).
38. Bărbulescu, A. Modeling the Greenhouse Gases Data Series in Europe During 1990–2021. *Toxics* **2023**, *11*, 726.
39. Bărbulescu, A. Statistical Analysis and Modeling of the CO_2 Series Emitted by Thirty European Countries. *Climate* **2024**, *12*, 34.
40. Eurostat. Greenhouse Gas Emissions by Source Sector (Table data series of all year). Available online: https://ec.europa.eu/eurostat/databrowser/view/env_air_gge__custom_12556357/default/table?lang=en (accessed on 22 October 2024).
41. Eurostat. Greenhouse Gas Emissions by Source Sector (Map for 2022). Available online: https://ec.europa.eu/eurostat/databrowser/view/env_air_gge__custom_14760995/default/map?lang=en (accessed on 22 October 2024).
42. 7.1.6. What are Outliers in the Data? Available online: https://www.itl.nist.gov/div898/handbook/prc/section1/prc16.htm (accessed on 22 October 2024).
43. Snedecor, G.W.; Cochran, W.G. *Statistical Methods*, 8th ed.; Iowa State University Press: Ames, IA, USA, 1989.
44. Pettitt, A.N. A non-parametric approach to the change-point problem. *J. R. Stat. Soc. Ser. C Appl. Stat.* **1979**, *28*, 126–135.
45. Conte, L.C.; Bayer, D.M.; Bayer, F.M. Bootstrap Pettitt test for detecting change points in hydroclimatological data: Case study of Itaipu Hydroelectric Plant, Brazil. *Hydrol. Sci. J.* **2019**, *64*, 1312–1326. https://doi.org/10.1080/02626667.2019.1632461.
46. Hubert, P. The segmentation procedure as a tool for discrete modeling of hydrometeorological regimes. *Stoch. Environ. Res. Risk A* **2000**, *14*, 297–304.
47. Page, E.S. Continuous Inspection Scheme. *Biometrika* **1954**, *41*, 100–115.
48. Gilbert, R.O. *Statistical Methods for Environmental Pollution Monitoring*; Van Nostrand Reinhold Company Inc.: New York, NY, USA, 1987. Available online: https://www.osti.gov/servlets/purl/7037501 (accessed 14 December 2024).
49. Bărbulescu, A.; Dumitriu, C.S. ARIMA and Wavelet-ARIMA Models for the Signal Produced by Ultrasound in Diesel. In Proceedings of the 25th International Conference on System Theory, Control and Computing (ICSTCC), Iasi, Romania, 20–23 October 2021; pp. 671–676.
50. Chakravarti, I.M.; Laha, R.G.; Roy, J. *Handbook of Methods of Applied Statistics*; John Wiley and Sons: Hoboken, NJ, USA, 1967; Volume I, pp. 392–394.
51. Anderson, T.W.; Darling, D.A. A Test of Goodness-of-Fit. *J. Am. Stat. Assoc.* **1954**, *49*, 765–769.
52. Brockwell, P.J.; Davis, R.A. *Time Series: Theory and Methods*, 2nd ed.; Springer: New York, NY, USA, 2009.
53. Bărbulescu, A.; Dumitriu, C.Ș. About the long-range dependence of cavitation effect on a copper alloy. *Rom. J. Phys*. **2024**, *69*, 904.
54. Dumitriu, C.Ș.; Dragomir, F.-L. Modeling the signals collected in cavitation field by stochastic and Artificial intelligence methods. In Proceedings of the 2021 13th International Conference on Electronics, Computers and Artificial Intelligence (ECAI), Pitești, Romania, 1–3 July 2021; pp. 1– 4.
55. Bărbulescu, A.; Dumitriu, C.Ș. Modeling the Voltage Produced by Ultrasound in Seawater by Stochastic and Artificial Intelligence Methods. *Sensors* **2022**, *22*, 1089.
56. Kwiatowski, D.; Phillips, P.C.B.; Schmidt, P.; Shin, Y. Testing the Null Hypothesis of Stationarity against the Alternative of a Unit Root. *J. Econom.* **1992**, *54*, 159–178.
57. Johnson, N.L.; Kotz, S.; Balakrishnan, N. *Continuous Univariate Distributions*; Wiley: New York, NY, USA, 1994; Volume 1, Chapter 12.
58. Kotz, S.; van Dorp, J.R. *Beyond Beta: Other Continuous Families of Distributions with Bounded Support and Applications*; World Scientific: Singapore, 2004.
59. Al Balasmeh, O.; Babbar, R.; Karmaker, T. Trend analysis and ARIMA modeling for forecasting precipitation pattern in Wadi Shueib catchment area in Jordan. *Arab. J. Geosci.* **2019**, *12*, 27.
60. Selvaraj, J.J.; Arunachalam, V.; Coronado-Franco, K.V.; Orjuela, L.V.R.; Yara, Y.N.R. Time-series modeling of fishery landings in the Colombian Pacific Ocean using an ARIMA model. *Reg. Stud. Mar. Sci.* **2020**, *39*, 101477.

61. Valipour, M.; Banihabib, M.E.; Behbahani, S.M.R. Comparison of the ARMA, ARIMA, and the autoregressive artificial neural network models in forecasting the monthly inflow of Dez dam reservoir. *J. Hydrol*. **2013**, *476*, 433–441.
62. Yu, Y.; Xie, Y.; Tao, Z.; Ju, H.; Wang, M. Global Temperature Prediction Models Based on ARIMA and LSTM. In *Image and Graphics Technologies and Applications. IGTA 2023*; Communications in Computer and Information Science; Yongtian, W., Lifang, W., Eds.; Springer: Singapore, 2023; Volume 1910.
63. Ryan, T.A.; Joiner, B.L. *Normal Probability Plots and Tests for Normality*; Technical Report; Statistics Department, The Pennsylvania State University: State College, PA, USA, 1976; pp. 1–7.
64. Levene, H. Robust Tests for Equality of Variances. In *Contributions to Probability and Statistics*, Olkin, I., Ed.; Stanford University Press: Palo Alto, CA, USA, 1960; pp. 278–292.